Shape phase transition and phase coexistence in odd Sm nuclei

Yu Zhang,[1] Feng Pan,[1,2] Yu-Xin Liu,[3,4] Yan-An Luo,[5] and J. P. Draayer[2]

[1]*Department of Physics, Liaoning Normal University, Dalian 116029, China*

[2]*Department of Physics and Astronomy, Louisiana State University, Baton Rouge, Louisiana 70803-4001, USA*

[3]*Department of Physics and the State Key Laboratory of Nuclear Physics and Technology, Peking University, Beijing 100871, China*

[4]*Center of Theoretical Nuclear Physics, National Laboratory of Heavy Ion Accelerator, Lanzhou 730000, China*

[5]*School of Physics, Nankai University, Tianjin 300071, China*

(Received 25 April 2013; revised manuscript received 11 June 2013; published 8 July 2013)

The shape phase transition and the associated phase coexistence in the odd Sm isotopes are investigated. Through analyzing two-neutron separation energies and the low-lying spectra of the odd Sm isotopes, it is found that the spherical to axially deformed shape phase transition does occur in the odd Sm nuclei just as their neighboring even Sm nuclei. The phase coexistence in ^{151}Sm, which lies close to the critical point, is revealed.

DOI: 10.1103/PhysRevC.88.014304 PACS number(s): 21.60.Fw, 21.60.Ev, 21.10.Re, 64.70.Tg

I. INTRODUCTION

Quantum phase transition is an interesting and important subject for many subfields. Atomic nuclei are good examples exhibiting quantum phase transitions in their isotope and isotone chains. The quantum phase transition is not of the usual thermodynamic type, but related to the equilibrium shape change in the ground state of nuclei at zero temperature, which is thus called shape phase transition (SPT). In the last ten years, a number of theoretical developments have provided new insights on understanding the evolution of nuclear structure in transitional regions through the SPT analysis [1–3].

For even-even nuclei, it is easy to identify the SPT by observing some typical quantities, such as the energy ratio $R_{4/2} = E_{4_1^+}/E_{2_1^+}$, the $E2$ transition rate $B(E2; 4_1^+ \to 2_1^+)$, the two-neutron separation energies, and so on, with variation of the mass number. An excellent example is provided by the even Sm isotopes, in which the structural evolution can be identified as the spherical to axially deformed SPT in experiment [4]. It is shown that the equilibrium shapes of ^{146,148}Sm may approximately be identified as spherical associated with the harmonic spectrum shown in their ground bands, and the shapes of ^{150,152}Sm seem relatively soft from their spectra, while the shapes of ^{154,156}Sm approach to axially deformed type associated with rotational spectra. The shape evolution with increasing of neutrons in Sm isotopes is thus identified as the first-order SPT, in which ^{150,152}Sm lie close to the critical point [5–8]. On the other hand, odd-A nuclei can be approximately considered as systems with an even-even core coupled to a single valence nucleon. Low-lying properties of odd-A nuclei should be impacted by the SPT emerging along the related odd isotope or isotone chains.

It is the purpose of this work to reveal whether the characters of the SPT in the adjacent even-even partners also emerge in odd Sm nuclei and how the SPT affect the properties of them. In Sec. II, the concept of the spherical to axially deformed SPT and the associated phase coexistence are introduced in the frame of the interacting boson model. Several analytically solvable collective modes within the Bohr-Mottelson model are also used to illustrate the structural evolution in the spherical to axially deformed SPT in even-even nuclei or that in the adjacent odd-A nuclei through the particle-core coupling scheme. In Sec. III, a parallel analysis of the SPT in the even and odd Sm nuclei is carried out. In Sec. IV, the phenomenon of phase coexistence in the odd Sm isotopes is revealed by comparison with the corresponding situation in the even Sm isotopes. A summary is given in Sec. V.

II. MODELS

A. Models of even-even nuclei

The interacting boson model (IBM) [4] and the Bohr-Mottelson model (BMM) [9] are two convenient models in analyzing SPT in nuclei. As an algebraic model, the IBM involves three dynamical symmetry limits, U(5), O(6), and SU(3) corresponding to a spherical vibrator, a γ-soft rotor, and an axially deformed rotor, respectively. Not only typical nuclei in these dynamical symmetry limit situations, but also those in the U(5)-SU(3) and the U(5)-O(6) transitional regions are observed experimentally [4]. In contrast to the IBM, the BMM is the geometric description of the above collective motions in nuclei. The IBM may be directly related to the BMM through the coherent state analysis [4,10].

In the IBM, to investigate the U(5)-SU(3) (the spherical to axially deformed) SPT, a schematic Hamiltonian may be written as [11]

$$\hat{H} = \varepsilon \left[(1-\xi)\hat{n}_d - \frac{\xi}{4N}\hat{Q}\cdot\hat{Q} \right], \tag{1}$$

where ε is a scale parameter, $\hat{n}_d = \sum_u d_u^\dagger d_u$ is the number operator of d bosons, and

$$\hat{Q}_\mu = (s^\dagger \times \tilde{d} + d^\dagger \times \tilde{s})^{(2)}_u - \frac{\sqrt{7}}{2}(d^\dagger \times \tilde{d})^{(2)}_u \tag{2}$$

is the quadrupole operator. Equation (1) can also be written as

$$\hat{H} = \varepsilon \left\{ (1-\xi)\hat{C}_1[\mathrm{U}(5)] - \frac{\xi}{8N}\left[\hat{C}_2[\mathrm{SU}(3)] - \frac{3}{4}\hat{C}_2[\mathrm{SO}(3)] \right] \right\}, \tag{3}$$

where $\hat{C}_k[\mathrm{G}]$ denotes the rank-k Casimir operator of group G [3,12]. It is clear that Eq. (3) is just the Hamiltonian in

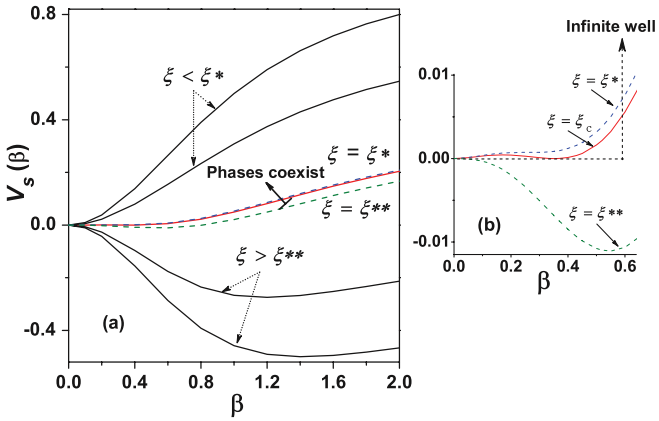

FIG. 1. (Color online) (a) The potential surfaces as functions of β with different ξ; (b) those at (ξ^*, ξ_c, ξ^{**}) on an expanded scale with the infinite well as approximation to the potential at ξ_c, where the γ variable has been frozen as $\gamma = 0$.

the U(5) limit when $\xi = 0$ and becomes that in the SU(3) limit when $\xi = 1$. For $\xi \in [0, 1]$, Eq. (3) can then be used to describe the U(5)-SU(3) (the spherical to axially deformed) transitional dynamics. Moreover, one may use the coherent state (also called the intrinsic state) defined as [4]

$$|\beta, \gamma, N\rangle = \frac{1}{\sqrt{N!(1+\beta^2)^N}}[s^\dagger + \beta\cos\gamma d_0^\dagger + \frac{1}{\sqrt{2}}\beta\sin\gamma(d_2^\dagger + d_{-2}^\dagger)]^N|0\rangle \quad (4)$$

to obtain the scaled potential surface corresponding to the Hamiltonian (1) or (3) in the large-N limit, which is

$$V_s(\beta, \gamma) = \frac{1}{\varepsilon N}\langle\beta, \gamma, N|H|\beta, \gamma, N\rangle|_{N\to\infty} = (1-\xi)\frac{\beta^2}{1+\beta^2} - \frac{\xi}{(1+\beta^2)^2} \times \left[\beta^2 + \frac{\sqrt{2}}{2}\beta^3\cos 3\gamma + \frac{1}{8}\beta^4\right]. \quad (5)$$

One can prove that the system experiences the first-order transition in the large-N limit as a function of ξ with the critical point $\xi_c = 8/17$, at which $V_{\min}$ [the minimum of $V_s(\beta, \gamma)$] is continuous, but $\frac{\partial V_{\min}}{\partial \xi}$ is discontinuous [4,11]. To understand the phase structure and the phase transition, we show the potential at different values of ξ in Fig. 1, where $\gamma = 0$ representing axially deformed situation is assumed since $V_{\min}(\beta)$ is always at $\gamma = 0$. As shown in panel (b) of Fig. 1, there are three important points in $V_s(\beta)$, the so-called spinodal point [11] $\xi^* = 0.47$, at which the second minimum of $V_s(\beta)$ appears, the critical point $\xi_c = 8/17$, at which the two minima of $V_s(\beta)$ are equivalent, and the antispinodal point $\xi^{**} = 0.5$, at which the first minimum of $V_s(\beta)$ disappears. Furthermore, one can find $V_{\min} = 0$ representing the spherical phase for $\xi < \xi^*$ and $V_{\min} < 0$ representing the deformed phase for $\xi > \xi_c$. Particularly, the narrow region with $\xi \in [\xi^*, \xi^{**}]$ shown in Fig. 1 is theoretically recognized as the phase coexistence region, in which the spherical and the axially deformed phases may coexist. The phase coexistence may be observed experimentally from quantities related to low-lying states of a nucleus [13]. Since the phase coexistence region defined above is just the narrow region involving the critical point as show in panel (a) of Fig. 1, it is also referred to as the critical region. Accordingly, the phase coexistence may be taken as an important signal to identify the critical nuclei along the related isotope or isotone chains with the first-order SPT.

In the BMM, on the other hand, the potential shown in Fig. 1 may be used to find a proper potential to describe the SPT in the model. With the shape variables β and γ, the BMM Hamiltonian is generally written as [9]

$$H_B = -\frac{\hbar^2}{2B}\left[\frac{1}{\beta^4}\frac{\partial}{\partial\beta}\beta^4\frac{\partial}{\partial\beta} + \frac{1}{\beta^2\sin 3\gamma}\frac{\partial}{\partial\gamma}\sin 3\gamma\frac{\partial}{\partial\gamma} - \frac{1}{4\beta^2}\sum_k\frac{\hat{L}_k^2}{\sin^2\left(\gamma - \frac{2}{3}\pi k\right)}\right] + V(\beta, \gamma), \quad (6)$$

where B is the the mass parameter, and $\hat{L}_k$ is the angular momentum operator expressed in the body-fixed frame. In the following, we will simply introduce several analytically solvable situations, from which the results may be taken as benchmarks for identifying typical structures appearing in the spherical-axially deformed SPT.

For a general form of $V(\beta, \gamma)$, one can only solve the corresponding BMM Hamiltonian numerically. However, there are some specific forms of $V(\beta, \gamma)$, for which one can find analytical solutions suitable to characterize the dynamical structure around the critical point resulting in the critical point symmetry (CPS) [14–16]. Specifically, the infinite square well was employed to simulate the flat potential at the critical point as shown in the right panel of Fig. 1, which results in the X(5) CPS [14] if assuming the potential $V(\beta, \gamma) = V(\beta) + V(\gamma)$ with $V(\gamma) \propto \gamma^2$, or the X(3) CPS [16] if assuming the γ degree of freedom frozen at $\gamma = 0$, while $V(\beta)$ was taken as

$$V(\beta) = \begin{cases} 0, & \beta \leqslant \beta_W, \\ \infty, & \beta > \beta_W, \end{cases} \quad (7)$$

for both the X(5) and X(3) cases. The levels of the yrast and yrare states in the X(5) and X(3) cases are mainly determined by the the radial part of the eigenequation:

$$\varphi''(z) + \frac{\varphi'(z)}{z} + \left[1 - \frac{v^2}{z^2}\right]\varphi(z) = 0, \varphi(k\beta_W) = 0, \quad (8)$$

with $v = \sqrt{\frac{L(L+1)}{3} + \frac{9}{4}}$ for the X(5) CPS and $v = \sqrt{\frac{L(L+1)}{3} + \frac{1}{4}}$ for the X(3) CPS, where $z = k\beta$ with $k = \sqrt{2BE/\hbar^2}$. The radial wave function $\varphi \propto J_v(k_{s,v}\beta)$ with $k_{s,v} = x_{s,v}/\beta_W$, where $x_{s,v}$ is the sth zero of the Bessel function $J_v(k_{s,v}\beta)$. The corresponding eigenenergy is $E = \frac{\hbar^2}{2B}(k_{s,v})^2$. The two CPS models can all be applied to describe even-even nuclei around the critical point of the spherical-axially deformed SPT. More discussions on the analytical solutions of the BMM with some other potentials may be found in [17].

In Table I, we list the normalized energy levels of the yrast states calculated from several collective modes corresponding to different deformed situations or shape phases in the SPT. As we know, the results of the IBM U(5) limit and the BMM with β^2 potential as well as those of the IBM SU(3) limit and the

TABLE I. The normalized low-lying yrast energy levels as functions of L produced by several typical collective models, where the ground state energy has been set to zero.

E_L	Vibrator	X(3) [16]	X(5) [14]	Rotor
E_2	1.00	1.00	1.00	1.00
E_4	2.00	2.44	2.91	3.33
E_6	3.00	4.23	5.43	7.00
E_8	4.00	6.35	8.48	12.00
E_{10}	5.00	8.78	12.03	18.33
E_{12}	6.00	11.52	16.04	26.00
E_{14}	7.00	14.57	20.51	35.00
E_{16}	8.00	17.91	25.44	45.33

BMM with β fixed as a nonzero value and γ frozen at $\gamma = 0$ representing axial symmetry [18], which just corresponds to the axial-symmetry rotor, are the same for the yrast states. For the case around the critical point, however, there is no simple correspondence between the IBM and the BMM. But the X(3) [16] or X(5) [14] CPS is effective for the description of the criticality of the spherical-axially deformed SPT. As shown in Table I, the spherical vibrator [or the IBM U(5) limit] produces equidistant yrast levels with $E_L = L/2$, and the axially deformed rotor [or the IBM SU(3) limit] provides yrast levels following the $L(L+1)$ law with $E_L = L(L+1)/6$, while, for given L, the X(5) or the X(3) model produces yrast level in between that of the vibrator and of the rotor following the relation $L/2 < E_L^{\mathrm{X(3)}} < E_L^{\mathrm{X(5)}} < L(L+1)/6$, which may be used to characterize the shape (phase) of a nucleus in this transitional region. Namely, a nucleus in this region with yrast levels obeying $E_L = L/2$ or $E_L = L(L+1)/6$ should be in the spherical vibrational or axially deformed phase, while that obeying $E_L^{\mathrm{X(3)}}$ or $E_L^{\mathrm{X(5)}}$ should be within the critical region of the spherical to axially deformed transition.

B. Particle-core coupling scheme for odd-A nuclei

As discussed previously, both the IBM and the BMM are suitable to describe the SPT in even-even nuclei. In contrast, there is lack of approach to describing structure of odd-A nuclei in a global way [19] due to diversity in their level structure. Even in the simplest model by considering the odd-A system as an even-even core plus a single particle [20], it is still difficult to find a way to describe low-lying structural evolution in the odd-A nuclei in a global way as done for the neighboring even-even nuclei. Nevertheless, one may figure out the main characters of the SPT in odd-A nuclei from some simple considerations. As is observed, spectrum in an odd-A nucleus in this region is mainly composed of $\Delta J = 1$ and $\Delta J = 2$ rotational-like bands, where J represents the quantum number of the total spin of each state in the band. If the coupling between the core and the single particle is not too strong, the intraband structure in the odd-A nuclei may be dominated by the collective motion of the core, while the single-particle excitation may only affect positions of band heads [20]. In this case, the $\Delta J = 2$ collective bands, of which the spectrum behaves similar to that of the even-even core, are favored in the low-lying part of the spectrum. This situation usually occurs to weakly or intermediately deformed nuclei [20,21]. When the coupling between the core and the particle is expected to be strong in a well-deformed situation, the $\Delta J = 1$ strong-coupling bands, which often follow the regular $J(J+1)$ rule, are favored in the low-lying part of the spectrum. For the spherical-axially deformed SPT, the weakly or intermediately deformed region just lies in between the spherical phase and the critical point. The well-deformed region is expected from the critical point to the axially deformed phase. In short, the results shown in Table I together with the $J(J+1)$ law may also be applicable to characterize the band structure and to identify the shape phase of odd-A nuclei in this region. The $\Delta J = 2$ and $\Delta J = 1$ collective bands in odd-A nuclei may be simply illustrated within the BMM in the weak-coupling limit, the decoupling limit, and the strong-coupling limit [20].

1. Weak-coupling limit

In the weak coupling limit, odd-A system may be approximately realized with the Hamiltonian

$$H_{\mathrm{odd}} = H_{\mathrm{coll}} + H_{\mathrm{sp}}, \tag{9}$$

where H_{coll} is the Hamiltonian of the collective core, and H_{sp} is that of the single particle. For simplicity, it is assumed that there is no additional interaction between the collective core and the particle in Eq. (9). For spherical or small deformation case, the collective part of the Hamiltonian H_{coll} may be chosen as Eq. (6), while the Hamiltonian for the single particle H_{sp} may be taken as that of the spherical shell model with

$$H_{\mathrm{sp}} = -\frac{\hbar^2}{2m}\nabla^2 + \frac{m\omega^2}{2}r^2 + C\hat{l}\cdot\hat{s} + D\hat{l}^2\,. \tag{10}$$

By solving the eigenequation $H_{\mathrm{odd}}\overline{\Psi} = E_{\mathrm{odd}}\overline{\Psi}$, it follows that the eigenfunction in the weak-coupling limit [20] can be constructed by coupling wave function of the collective-core with that of the single-particle in the spherical form as

$$\overline{\Psi} = \sum_{M_L, m_j} < L, M_L; j, m_j | J, M_J > \Psi_{L,M_L}(\beta,\gamma,\theta)\chi_{j,m_j}(\eta), \tag{11}$$

where $\chi_{j,m_j}(\eta)$ is the single particle wave function satisfying

$$H_{\mathrm{sp}}\chi_{j,m_j}(\eta) = e_j\chi_{j,m_j}(\eta) \tag{12}$$

with η representing generically the coordinates of the single particle [22–25], and $\Psi_{L,M_L}(\beta,\gamma,\theta)$ is the wave function describing the collective core satisfying

$$H_{\mathrm{coll}}\Psi_{L,M_L}(\beta,\gamma,\theta) = E_{\mathrm{coll}}\Psi_{L,M_L}(\beta,\gamma,\theta)\,. \tag{13}$$

Then the total energy is given as

$$E_{\mathrm{odd}} = E_{\mathrm{coll}} + e_j\,. \tag{14}$$

It is clear that the E_{coll} describes the collective excitations, and e_j describes the single-particle excitations. In this case, the collective bandheads are determined by the single-particle excitations, and the intraband level spacings are determined by the collective excitations. Therefore, the single-particle energy e_j in Eq. (14) is simply adjusted to align with the bandhead with $J = j$ determined from experiment. In this

scheme, the states with the total spin given as $J = |L - j|, |L - j| + 1, \ldots, L + j$ are degenerate and show the same spectral structure as that of the core with the same orbit angular momentum quantum number L. Especially, the levels in the $\Delta J = 2$ collective band with the spin sequence $J = j, j + 2, j + 4, \ldots$, described by $H_{\rm odd}$ may behave the same as those in the ground band of the even-even system described by $H_{\rm coll}$. As a result, the quantities listed in Table I can be used to characterize either the yrast levels with angular momentum L of the even-even nuclei or those with $J = j + L$ in the neighboring odd-A nuclei.

In odd-A nuclei, spins of bandheads in some $\Delta J = 2$ collective bands may be not $J = j$, but $J = j - n$ with $n = 1, 2, \ldots, j - 1/2$, which may be explained by taking into account the additional interactions between the core and the odd particle. This bandhead spin assignment is assumed in the weak-coupling limit in this work by considering $j' = j - n$ as the effective spin of the single particle. Thus, the spectral characters of the collective bands in odd-A nuclei with spin $J = j - n + L$ and $n = 0, 1, 2, \ldots, j - 1/2$ described by $H_{\rm odd}$ in the weak-coupling limit are almost the same as those of the ground band of the even-even nuclei described by $H_{\rm coll}$. It should be emphasized that some model features may be unrealistic, such as degeneracy in states with the same L in the weak-coupling limit mentioned previously. The weak-coupling limit of the BMM is just used to illustrate the structural evolution of the $\Delta J = 2$ band and the SPT in in the odd-A nuclei.

2. Decoupling limit

As shown in [26], the $\Delta J = 2$ collective bands in an intermediately deformed odd-A nucleus with an even-even core around the critical point may be described within the decoupling scheme, in which the Hamiltonian and wave function of the single particle should be expressed in the intrinsic frame of the deformed core described by the corresponding CPS. Then the Hamiltonian of the odd-A nucleus in the decoupling limit can be written as the same form given in Eq. (9) but with

$$H_{\rm coll} = H_{\rm CPS} \tag{15}$$

and

$$H_{\rm sp} = H_{\rm sph} + k\beta_0 Y_{20}(\theta', \phi'), \tag{16}$$

where $H_{\rm CPS}$ is the corresponding CPS Hamiltonian describing the collective core, and $H_{\rm sp}$ is the single-particle Hamiltonian, in which the first term $H_{\rm sph}$ is the part in the spherical shell model the same as that given in Eq. (10) and the second term represents a quadrupole field oriented along the core symmetry axis z [20,21,26]. For a given Ω, which is the projection of j on the z axis, eigenvalue of $H_{\rm sp}$ under the single-particle wave function $|\chi^j_\Omega(\eta)\rangle$ is given by

$$\begin{aligned} E_{\rm sp} &\approx e_j + k\beta_0 \left(\frac{3\Omega^2 - j(j+1)}{4j(j+1)}\right) \\ &= e'_j + \frac{3k\beta_0}{4j(j+1)}\Omega^2 . \end{aligned} \tag{17}$$

It is realized [20,21] that the core may decouple from the single particle if the angular momentum of the particle is aligned along the rotational axis, which may occur due to the fact that there is a cancellation of the Ω dependent term coming from the intrinsic part as described by the second term in Eq. (17) and that coming from the so called recoil term $-\frac{1}{\Gamma}\hat{J}_z\hat{j}_z$ involved in $\frac{1}{\Gamma}\hat{L}^2 = \frac{1}{\Gamma}(\hat{J} - \hat{j})^2$ included in the CPS Hamiltonian for the axially symmetric system, where Γ is a model-dependent inertial parameter. A detailed derivation on the decoupling conditions for the X(3) CPS is given in [26]. It is shown in [26] that the resulting levels in each collective band should be characterized with $\Delta J = 2$ in the decoupling limit due to the reflection symmetry in the plane perpendicular to the symmetry axis [20,21]. These levels behave the same as those in the ground band of the even-even core described by the X(3) CPS. Actually, the same spectral characters also emerge in energy levels of the so called favorite states with $J = j, j + 2, j + 4, \ldots$, in the weak-coupling scheme [20]. Anyway, the results of the decoupling limit further confirm that the low-lying level scheme of a weakly or intermediately deformed odd-A nucleus is indeed dominated by the $\Delta J = 2$ collective bands with level structure similar to that of the core. In addition, the similar results can also be obtained from the coupling scheme shown in [26] with the X(5) CPS core.

3. Strong-coupling limit

In the well-deformed situation, the particle-rotor model in the strong-coupling limit [20] is a suitable scheme to describe the low-lying dynamics of odd-A nuclei. In this case, the collective part in Eq. (9) may be taken as the Hamiltonian of the symmetric rotor,

$$H_{\rm coll} = H_{\rm rot} = \frac{\hbar^2}{2\Gamma}\hat{L}^2 + \frac{\hbar^2}{2\Gamma_{z'}}\hat{L}^2_{z'} \tag{18}$$

with $\hat{L} = \hat{J} - \hat{j}$, while the single-particle part may be taken as that of the deformed shell model with

$$H_{\rm sp} = H_K = \sum_i E^i_{K_i} f^\dagger_{iK_i} f_{iK_i}, \tag{19}$$

where $f^\dagger_{iK_i}$ (f_{iK_i}) is the creation (annihilation) operator of the valence particle in the ith Nilsson orbit [20], and $E^i_{K_i}$ is the corresponding single-particle energy. By ignoring the rotor-particle coupling term, the total wave function in the strong-coupling limit after symmetrization can be analytically written as

$$\begin{aligned} \Psi'_{JMK} = \sqrt{\frac{2J+1}{16\pi^2}} \big[& D^J_{M,K}(\theta_k)|\phi_K\rangle \\ & + (-)^{J+K} D^J_{M,-K}(\theta_k)|\phi_{\bar{K}}\rangle \big], \end{aligned} \tag{20}$$

where the $D^J_{M,K}(\theta_k)$ is the Wigner D function satisfying

$$H_{\rm rot} D^J_{M,K}(\theta_k) = \left[E'_K + \frac{\hbar^2}{2\Gamma}J(J+1)\right] D^J_{M,K}(\theta_k), \tag{21}$$

where E'_K is related to the quantum number K, and $J = K, K + 1, K + 2, K + 3, \ldots$. In addition, $|\phi_K\rangle$ in Eq. (20)

is the single-particle wave function satisfying

$$H_K|\phi_K\rangle = E_K|\phi_K\rangle\,. \tag{22}$$

Then the total energy of the system is given by

$$E = E_K + E'_K + \frac{\hbar^2}{2\Gamma}J(J+1)\,. \tag{23}$$

The first two terms in Eq. (23) are often adjusted to fit the bandhead energy of each strong-coupling band according to experimental data since K is a good quantum number in an axial system, while the last term describes the intraband rotational excitations, which clearly falls into the $J(J+1)$ rule.

III. THE SPT AND SPECTRAL EVOLUTION IN SM NUCLEI

The two-neutron separation energy S_{2n} may be considered as a primary and direct signature of the emergence of SPT [1,4]. In the IBM [1,27], S_{2n} with $S_{2n} = -[E_0(N-1) - E_0(N)]$ is related to the derivative $\frac{\partial E_0}{\partial \xi}$ of the relevant ground state energy E_0 with respect to the control parameter ξ. In the large-N limit, using the result of the coherent state theory, one can find $\frac{\partial E_0}{\partial \xi} \propto \frac{\partial V_{\rm min}}{\partial \xi}$, which can be directly calculated from Eq. (5). In the finite-N case of the IBM, S_{2n} may be written as a smooth contribution linear with the boson number N plus contribution from the deformation [4,27,28]

$$S_{2n} = -A - BN + S(2n)_{\rm def}\,. \tag{24}$$

Similar to the analysis shown in [27], we focus on the deformation contribution, which is obtained from the data by subtracting a term linear with the total number of valence nucleon pairs. Accordingly, the experimental values of $S(2n)_{\rm def}$ for both the even and odd Sm nuclei as functions of N_ν are shown in Fig. 2, where N_ν is the neutron boson number taken as the number of valence neutron pairs since the proton number is a constant with $n_\pi = 62$. The results are obtained from the data [29–40] fitted with $A = -19.768$ and -19.378 MeV for the even and odd Sm nuclei, respectively, and $B = 0.658$ MeV according to Eq. (24). Concretely, we use the linear function $f(N) = -A - BN$ to fit the experimental values of S_{2n} for the spherical-like nuclei ^{144,146,148}Sm as well as their odd-neutron partners to fix A and B since S_{2n} in these spherical-like nuclei indeed behaves as a linear function of the number of valence nucleons [2]. Then, one can get $S(2n)_{\rm def}$ by subtracting the linear part calculated with $f(N)$ from the experimental value of S_{2n} according to (24). It should be noted that $S(2n)_{\rm def}$ of the even Sm nuclei and their odd-proton partners, Eu, were discussed in [27], in which the linear function $f(N_\nu) = -A - BN_\nu$ was used. As shown in Fig. 2, the evident SPT signal in $S(2n)_{\rm def}$ can be observed around $N_\nu = 4$ for both the even and odd Sm isotopes. Particularly, the effect of the additional neutron seems to enhance the character of SPT in the odd Sm nuclei, in which the amplitude of $S(2n)_{\rm def}$ increases about 1/4 near the critical point in comparison to that in the even nuclei. According to the theoretical prediction in the large-N limit of the IBM, which basically agrees with the experimental results [27] as shown in the inset of Fig. 2, the

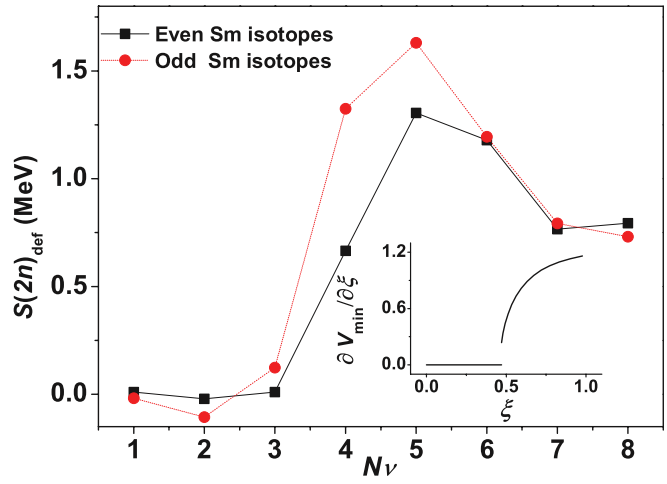

FIG. 2. (Color online) The contribution of deformation to the two-neutron separation energies, $S(2n)_{\rm def}$ (in MeV) for both the even and odd Sm isotopes, plotted as a function of neutron boson number, N_ν. The contribution is enhanced about 330 keV at $N_\nu = 5$ in the odd Sm nuclei. Also the increase of $S(2n)_{\rm def}$ from $N_\nu = 3$ to $N_\nu = 4$ is sharper in the odd Sm nuclei than that in the even Sm nuclei. In the $N \to \infty$ limit of the IBM [27], $S(2n)_{\rm def}$ should be zero when $\xi \leqslant \xi_c$ and finite but large when $\xi > \xi_c$. The expected behavior of $-\frac{\partial V_{\rm min}}{\partial \xi}$ is shown in the inset. The experimental data are taken from [29–40].

spherical to axially deformed SPT emerging in ground state of the Sm nuclei with the critical point around $N_\nu = 4$ is of the first order.

The above analysis shows that the SPT indeed emerges at the ground states of the odd Sm nuclei as that emerging in the adjacent even Sm nuclei. It is expected that a parallel description of the SPT for both the even and odd Sm isotopes is possible. As shown in the previous section, the characters of SPT are not only reflected in ground state of a nucleus, but also in its low-lying spectrum, which has been widely confirmed in even-even nuclei [1,2]. However, spectra of odd-A nuclei often involve both collective and single-particle excitations, which are much more complex than those of even-even nuclei. But the low-lying spectral behaviors in the odd Sm nuclei seem more "regular" than expected, which provide a rare chance to probe the SPT in low-lying spectra of odd-A nuclei.

In the following, we consider the ground bands for both the even and the odd Sm nuclei, of which the lowest excited bands are also taken into account. In Fig. 3, the normalized experimental energy levels of the Sm nuclei and the theoretical results of several models provided in Table I as functions of L in both the ground and first excited bands are shown to illustrate the SPT. Since we only emphasize their band structure, all bandhead energies have been set to zero, with which other levels are normalized to the first excited level in each band. In the even Sm nuclei, the results shown from Fig. 3 indicate that the ground band, as expected, evolve from the vibrational type in ^{146,148}Sm to the rotational type in ^{154,156}Sm with increasing of neutrons, which clearly reflects the SPT from the spherical to the axially deformed shape with ^{150,152}Sm around the critical point [5,7,8], which is consistent with the SPT prediction shown by the contribution of deformation to the two-neutron separation energy $S(2n)_{\rm def}$ related to their ground

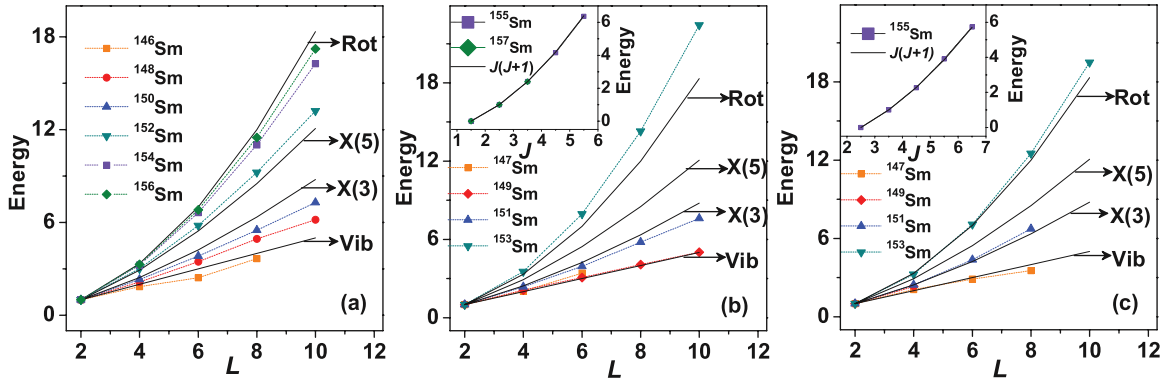

FIG. 3. (Color online) (a) The normalized experimental energy levels of the ground bands of the even Sm nuclei together with those calculated by several typical collective models shown in Table I, in which Rot represents the results of the Rotor, Vib corresponds to the results of the Vibrator, and X(3), and X(5) represent those given by the X(3) and the X(5) CPS [14,16]; (b) the same as (a) but for the ground band of the odd Sm nuclei, where Vib, X(3), X(5), and Rot represent the results of the corresponding collective modes in the weak-coupling limit, which are actually the same as those list in Table I according to the discussion in Sec. II, and the subpanel shows the spectra of ^{155,157}Sm together with those following the $J(J+1)$ law solved from the particle-rotor model in the strong-coupling limit; (c) the same as those in (b) but for the first excited band of the odd Sm nuclei. It should be note that all the bandhead energies have been set to zero, and the levels in the band with $\Delta J = 2$ are normalized to the levels with $J = J_0 + 2$, while the levels in the band with $\Delta J = 1$ are normalized to the levels with $J = J_0 + 1$, where $L = J - J_0$ with J being the total spin of the level and J_0 being the spin of the band head. The experimental data are taken from [29–40].

states. Moreover, it can be observed from panels (a) and (b) of Fig. 3 that the structural evolution of the ground bands of the odd Sm nuclei and that of the even Sm nuclei with variation of neutron number are quite similar. Specifically, ^{147,149}Sm may correspond to the spherical shapes with the vibrational character in their ground bands. ^{155,157}Sm may be related to the axially deformed shapes with their ground bands obeying the $J(J+1)$ rotational rule in the strong-coupling limit. ^{151}Sm may be associated with a soft shape with its ground band following the X(3)-like results. However, the ground band of ^{153}Sm shows a rotational-like spectrum obeying the $L(L+1)$ law as shown in Fig. 3, where L is the angular momentum quantum number of the core, while its even partner ^{152}Sm presents a relatively softer ground band structure characterized by the X(5) CPS. It seems that the dynamics around the critical point are evidently impacted by the additional neutron, which leads to the shape of the odd-A nucleus more rigid than expected. In addition, the evolution pattern of the first excited bands in the odd Sm isotopes is similar to that of the ground bands as shown in panel (c) of Fig. 3. The levels in the first excited band of ^{153}Sm also obey the $L(L+1)$ law as those in the ground band. It should be noted the the two rotational-like bands with $\Delta J = 2$ in ^{153}Sm shown in panels (b) and (c) are often treated together as a single strong-coupling rotational band [36] with $\Delta J = 1$. Further discussion about this will be shown in Sec. IV. Generally, the strong-coupling dynamics results in a more deformed situation. As a result, no matter whether it is considered as the single strong-coupling band or two rotational-like bands, the spectrum in ^{153}Sm shown in Fig. 3 reflects the fact that it is more rigid with larger deformation than ^{151}Sm. Therefore, with increasing of neutrons, the low-lying band structures of the odd Sm isotopes all evolve from the vibrational type with $\Delta J = 2$ to a soft type with $\Delta J = 2$, then to a little rigid type with $\Delta J = 2$ or $\Delta J = 1$ undetermined, and finally to the strong-coupling rotational type with $\Delta J = 1$. Thus, the spherical to axially deformed SPT in the odd Sm nuclei is indeed reflected from their low-lying spectra, in which both the collective mode and the coupling of the collective core with the single neutron seem subject to change during the SPT.

In addition, the properties of $E2$ transition may be also used to indicate the occurrence of shape phase transition. However, there is no sufficient experimental $B(E2)$ data for the odd Sm nuclei to show the actual evolution of the ground band. Therefore, we may focus on discussing the properties of the low-lying energies for the odd Sm nuclei in the present work.

IV. THE PHASE COEXISTENCE IN SM NUCLEI

Another important phenomenon closely related to the first-order SPT is that the phase coexistence may occur to the low-lying states of the nuclei around the critical point according to the theoretical discussions shown in Sec. II. The analysis shown in [13] indicate that the phase coexistence may occur to the transitional nucleus ^{152}Sm, which may be the best candidate of the X(5) CPS [1,6].

To illustrate this phenomenon in the transitional region of the even Sm isotopes, the energy levels in the ground band and the β band of both ^{150}Sm and ^{152}Sm are shown in Fig. 4. It can be seen from panel (a) of Fig. 4 that the levels in both the ground band and the β band of ^{150}Sm behave as an anharmonic vibrator with $R_{4/2} \approx 2.3$. There is no clear sign of phase coexistence in its low-lying states though it is near the critical point and expected to be the candidate as analyzed in [7]. In contrast, the ground band of ^{152}Sm shows a rotational character with $R_{4/2} = 3.00$, while the β band seems vibrational with $R_{4/2} = 2.7$ as shown in panel (b) of Fig. 4. The signal of the spherical and the deformed

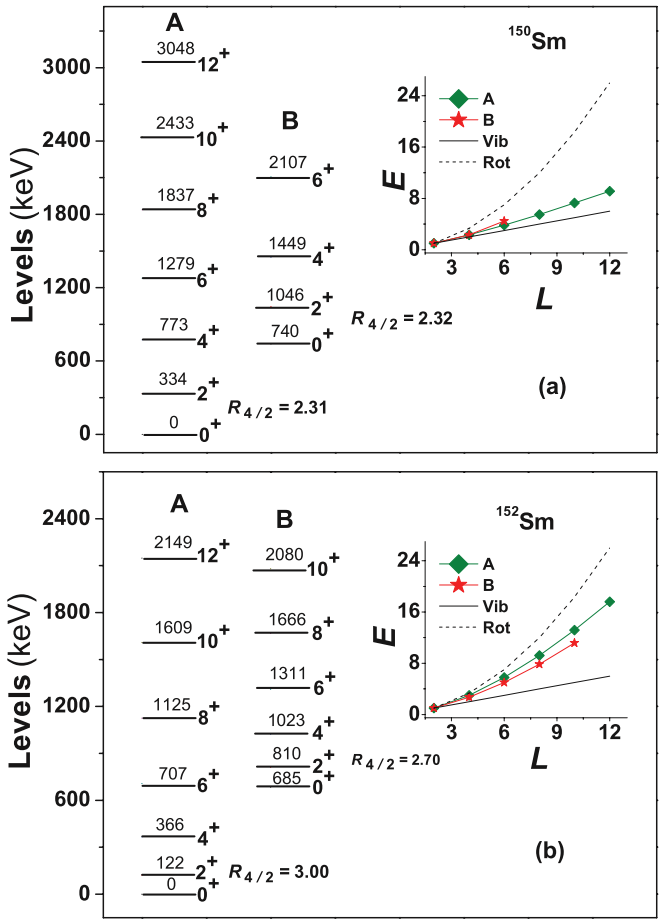

FIG. 4. (Color online) The experimental energy levels in the ground band and the β band of ^{150}Sm and those of ^{152}Sm. The corresponding normalized results are shown in the insets, where the theoretical results of rotor and vibrator are also given to compare the experimental behaviors. The experimental data are taken from [33,35].

phase coexisting in ^{152}Sm highlighted by distinct $R_{4/2}$ ratios in the two bands was thus identified in the analysis [13]. In addition, the vibrational character of the β band in ^{152}Sm may also be tracked by the fact that the 4^+ level at 1023 keV in the β band shown in panel (b) is approximately degenerated with the 0_3^+ level at 1083 keV and the 2_3^+ level at 1086 keV, which is consistent with the vibrational U(5)-like spectrum [4]. Moreover, the experimental $B(E2)$ ratios of ^{152}Sm, especially $B(E2;2_3^+ \to 0_2^+)/B(E2;2_1^+ \to 0_1^+)$, also follow the phase coexistence prediction according to the discussions shown in [13,41,42], though different view also exists [43], in which the author considered the ground state and 0_2^+ state in ^{152}Sm as shape coexisting states. However, though the distinction from such shape coexistence and the phase coexistence of the X(5) description is subtle [1,44,45], more experimental and theoretical study are needed [46] in order to make a conclusion.

It should be emphasized that one can discriminate in principle between a region in which phase transitions occur and a region that exhibits shape coexistence as discussed in [44]. It is pointed out [44] that in the case of phase transitions the two different types of motion can only develop resembling the motion generated by H_1 and H_2, where the Hamiltonian H_1 and H_2 describe two different types of motion that are basically incompatible with one another [e.g., the two terms given in Eq. (1)]. In such case, it is clear that both Hamiltonian work in the same Hilbert space, namely $\Phi = \Phi_1 = \Phi_2$ [44]. On the other hand, when shape coexistence appears, complete sets of states can be generated in each space, and the dynamical structure is determined by the direct product of the Hilbert spaces describing the various phases like $\Phi_1 \otimes \Phi_2 \otimes \Phi_3 \ldots$ [44]. Here, we do not emphasize the difference of the phase coexistence from the shape coexistence, but follow the phase coexistence concept to illustrate the phenomenon that several collective bands with different intraband structures may coexist in the low-lying spectrum of the critical point nucleus. It will be shown that the coexistence of several collective bands of different types in the low-lying spectrum may be the unique phenomenon emerging only around the critical point in the odd Sm nuclei, which indicates that this character can indeed be manifested by the SPT.

To reveal the phase coexistence in the odd Sm nuclei, several low-lying bands of both ^{151}Sm and ^{153}Sm are shown in Fig. 5, where the low-lying band is the band with its bandhead energy less than 0.5 MeV for odd-A nuclei. It can be clearly seen from panel (a) of Fig. 5 that the levels in the ground band labeled with A and those in the first excited band labeled with B behave more or less soft in between the vibrational and rotational, and the levels in the second excited band labeled with C follow vibrational pattern, while those in the band labeled with D follow the strong-coupling $J(J+1)$ rotational rule. Thus, the vibrational and rotational phases clearly coexist in the low-lying spectrum of ^{151}Sm. In addition, one can see that the spin and parity of the bandhead of band C is $J^\pi = 7/2^-$, which shows that the final valence neutron in ^{151}Sm may occupy the $2f_{7/2}$ orbit [34] in the first single-j shell after the magic number $N = 82$. In fact, the spins and parities of the bandheads of the ground band in both ^{147}Sm [30] and ^{149}Sm [32] are also $J^\pi = 7/2^-$. It is a common character that all these bands are of vibrational type. Therefore, these vibrational bands may all built on the same single-particle orbit $2f_{7/2}$ no matter whether they are ground or excited bands. It is shown in panel (b) of Fig. 5 for ^{153}Sm that the parities of band A and B are all positive, in which the levels approximately follow the $L(L+1)$ law, while band C and D with negative parity obviously follow the strong-coupling $J(J+1)$ law. Therefore, all the low-lying bands in ^{153}Sm are almost rotational. It should be noted the two $\Delta J = 2$ positive parity band A and B in ^{153}Sm are often treated as the single $\Delta J = 1$ strong-coupling rotational band [36] built on the mixed $3/2^+[651] + 3/2^+[402]$ single-particle state with the strong Coriolis coupling between the ground state and the excited positive-parity orbits in the $i_{13/2}$ shell [47]. Nevertheless, the strong-coupling perspective seems difficult to explain the two rotational-like bands shown in Fig. 5, especially the excited band B shown in panel (b), in which the energy levels follow the $L(L+1)$ law from $J^\pi = 5/2^+$ to $J^\pi = 37/2^+$ with deviation less than 7%. Besides, the first $J^\pi = 5/2^+$ level with $E_{5/2^+} = 7.535$keV [36] is too close to

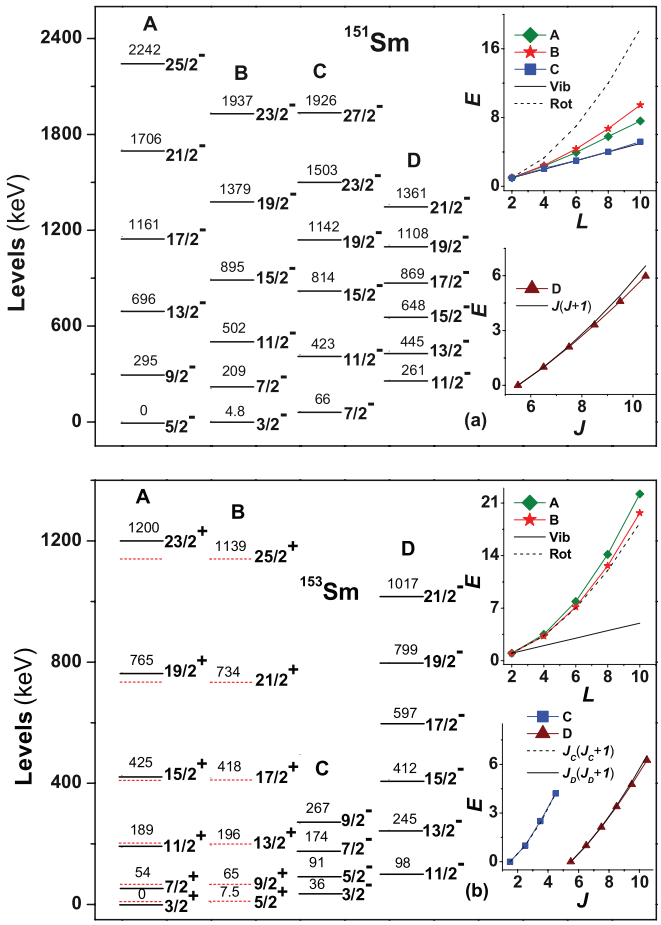

FIG. 5. (Color online) (a) The experimental energy levels of the lowest three $\Delta J = 2$ collective bands and the lowest $\Delta J = 1$ negative parity band in ^{151}Sm and the subpanels showing the normalized results with $L = J - J_0$ and J_0 being the spin of bandhead as in Fig. 3. (b) Similar to those in (a) but for the experimental energy levels of the lowest four collective bands in ^{153}Sm. The $\Delta J = 2$ band denoted by A (short solid lines) and the one denoted by B (short dash lines) are often explained as the single $\Delta J = 1$ strong-coupling band with the levels signified by the short solid and dash lines together under A. The experimental data shown (a) and (b) are taken from [34,36].

the ground level to be considered as the first excited rotational level in the ground band. Moreover, the increasing ordering of spin of the states in the ground band will no longer be valid after $J^\pi = 13/2^+$ if these levels are treated as those in the single $\Delta J = 1$ rotational band shown by the short dashed and solid lines under the label A. Therefore, it seems more reasonable that these positive parity levels come from two regular rotational-like bands rather than the highly irregular single $\Delta J = 1$ band, which may further be verified by $E2$ transition from the $J^\pi = 5/2^+$ state to the ground state, but there has been no experimental result available.

On the other hand, the strong-coupling rotational band with spin and parity of the bandhead $J_0^\pi = 3/2^-$ built on $3/2^-[521]$ is favored in Sm isotopes for $A > 151$. Specifically, this band appears as the first excited negative parity band of ^{153}Sm, but as the ground band of both ^{155}Sm and ^{157}Sm. In addition, another strong-coupling rotational band with spin and parity of the bandhead $J_0^\pi = 11/2^-$ built on $11/2^-[505]$ appears in both ^{151}Sm and ^{153}Sm, which indicates that the deformation becomes energetically favored around the critical point. It should be noted that the strong coupling band built on $11/2^-[505]$ also appears in ^{149}Sm but with the bandhead energy higher than 1.3 MeV. Therefore, the low-lying structure of ^{149}Sm is still dominated by the vibrational modes. Based on the discussions shown in Sec. II, it is easy to explain the $\Delta J = 1$ strong-coupling bands built on the corresponding Nilsson single-particle orbit in the particle-rotor model [20], of which the physical picture seems valid in the well-deformed situation. In contrast, the $\Delta J = 2$ bands are often related to the spherical or weakly deformed situation, which results from the corresponding single-particle excitations of the spherical shell model. Thus, one can conclude for the odd Sm nuclei that the spherical vibrational phase built on $2f_{7/2}$ orbit may dominate in the ground state when $A < 151$; the vibrational and the rotational phases coexist in the low-lying spectrum at $A = 151$; the rotational phase built on several deformed single-particle orbits begin to dominate in the low-lying spectrum of ^{153}Sm; and the rotational phase built on $3/2^-[521]$ dominate in the ground state when $A > 153$.

Comparatively speaking, the characters of the phase coexistence shown in ^{151}Sm are much clearer and richer than those shown in ^{152}Sm. The origination of the phase coexistence due to the competition between the spherical vibrational and the deformed rotational phase is also more explicitly shown in the former. On the other hand, it was recognized [1,2] that collective phenomena in nuclei may be due to competition between the spherical-driving pairing interaction and the deformation-driving valence proton-neutron interaction. Though the neutron-proton interaction is not considered explicitly in our analysis, it is certainly included in both the IBM-1 and the collective model shown in Sec. II as justified in [48]. The difference of the phase coexistence in the odd Sm nuclei from that in the even Sm nuclei is also shown. The bandheads of the collective bands in the former are determined by single-particle excitations, but those in the latter may originate from the collective excitations.

V. SUMMARY AND CONCLUSION

In summary, the SPT in the odd Sm nuclei has been investigated through the parallel analysis of the even Sm nuclei. It is found that the SPT indeed occurs in the odd Sm isotopes. The signals of the SPT are even enhanced by the effects due to the additional single particle of the odd Sm nuclei in comparison to the even Sm isotopes. Our analysis on the spectral evolution shows that the SPT in odd Sm nuclei is the spherical to the axially deformed shape phase transition, of which the basic characters are quite similar to those appearing in the even Sm nuclei. More importantly, it is shown that the phenomenon of the phase coexistence also emerges in the critical region of odd Sm nuclei, especially in ^{151}Sm, just as that emerging in the even Sm isotopes [13], but with more signals. Concretely, it is clearly shown that the regular vibrational bands and strong-coupling rotational bands together with the anharmonic vibrational or softly rotational bands in between

them may coexist in the low-lying spectrum of ^{151}Sm, which is explained in terms of the vibrational phase and rotational phase coexistence around the critical point caused by the SPT. Our present analysis not only shows the clear evidence of the SPT, but also reveals that the phenomenon of phase coexistence and the low-lying structural evolution due to the SPT may be related in these odd-A nuclei. It seems that the low-lying dynamical evolution in the odd Sm nuclei can be qualitatively illustrated with the help of several simple collective models. However, since the models of odd-A nuclei presented in Sec. II are quite simple, some features predicted may be unrealistic. For example, the degeneracy of several states with the same L appearing in the weak-coupling limit should be removed. Therefore, further improvement by considering interactions between the core and the particle is necessary in order to describe energy levels and electromagnetic properties of these nuclei in quantity. Recently, some attempts [27,49,50] in elucidating the SPT in odd-A nuclei have also been made in the interacting boson-fermion model (IBFM) [51]. In contrast to the previous theoretical analysis on the SPT in odd-A nuclei [52–56], the evolution of deformation and spectra based on the unique parity configuration $h_{11/2}$ in some odd-proton nuclei were studied [27,49,50]. Especially, the recent studies [57] show that the low-lying spectrum of the odd Pm isotopes can be well described within the framework of the neutron-proton IBFM. It is expected that the IBFM after some reformulation may be suitable to describe low-lying spectra and structural evolution of these odd-A nuclei quantitatively in a global way just as done by the IBM for even-even nuclei. Related work is in progress.

ACKNOWLEDGMENTS

Support from the US National Science Foundation (OCI-0904874), the Southeastern Universities Research Association, the Natural Science Foundation of China (11005056, 11175078, 11075080, 10935001, and 11075052), the Major State Basic Research Development Program (G2007CB815000), the Doctoral Program Foundation of State Education Ministry of China (20102136110002), and the LSU–LNNU joint research program (9961) is acknowledged.

[1] P. Cejnar, J. Jolie, and R. F. Casten, Rev. Mod. Phys. **82**, 2155 (2010).
[2] R. F. Casten and E. A. McCutchan, J. Phys. G **34**, 285 (2007).
[3] P. Cejnar and J. Jolie, Prog. Part. Nucl. Phys. **62**, 210 (2009)
[4] F. Iachello and A. Arima, *The Interacting Boson Model* (Cambridge University Press, Cambridge, 1987).
[5] R. F. Casten, D. Kusnezov, and N. V. Zamfir, Phys. Rev. Lett. **82**, 5000 (1999).
[6] R. F. Casten and N. V. Zamfir, Phys. Rev. Lett. **87**, 052503 (2001).
[7] J. E. García-Ramos, J. M. Arias, J. Barea, and A. Frank, Phys. Rev. C **68**, 024307 (2003).
[8] J. Meng, W. Zhang, S. Q. Zhang, H. Toki, and L. S. Geng, Eur. Phys. J. A **25**, 23 (2005).
[9] A. Bohr and B. R. Mottelson, *Nuclear Structure*, Vol. 2 (World Scientific, Singapore, 1998).
[10] J. N. Ginocchio and M. W. Kirson, Nucl. Phys. A **350**, 31 (1980).
[11] F. Iachello and N. V. Zamfir, Phys. Rev. Lett. **92**, 212501 (2004).
[12] Y. Zhang, F. Pan, Y. X. Liu, Y. A. Luo, and J. P. Draayer, Phys. Rev. C **85**, 064312 (2012).
[13] F. Iachello, N. V. Zamfir, and R. F. Casten, Phys. Rev. Lett. **81**, 1191 (1998).
[14] F. Iachello, Phys. Rev. Lett. **85**, 3580 (2000); **87**, 052502 (2001); **91**, 132502 (2003).
[15] Dennis Bonatsos, D. Lenis, D. Petrellis, and P. A. Terziev, Phys. Lett. B **588**, 172 (2004).
[16] Dennis Bonatsos, D. Lenis, D. Petrellis, P. A. Terziev, and I. Yigitoglu, Phys. Lett. B **632**, 238 (2006); **621**, 102 (2005).
[17] L. Fortunato, Eur. Phys. J. A **26**, 1 (2005).
[18] N. Pietralla and O. M. Gorbachenko, Phys. Rev. C **70**, 011304(R) (2004).
[19] D. Bucurescu, G. Căta-Danil, M. Ivascu, L. Stroe, and C. A. Ur, Phys. Rev. C **49**, R1759 (1994).
[20] P. Ring and P. Schuck, *The Nuclear Many-Body Problem* (Springer-Verlag, Berlin, 1980).
[21] F. S. Stephens, Rev. Mod. Phys. **47**, 43 (1975).
[22] F. Iachello, Phys. Rev. Lett. **95**, 052503 (2005).
[23] C. E. Alonso, J. M. Arias, and A. Vitturi, Phys. Rev. Lett. **98**, 052501 (2007).
[24] Y. Zhang, F. Pan, Y. X. Liu, Z. F. Hou, and J. P. Draayer, Phys. Rev. C **82**, 034327 (2010).
[25] Y. Zhang, F. Pan, Y. X. Liu, Y. A. Luo, and J. P. Draayer, Phys. Rev. C **84**, 034306 (2011).
[26] Y. Zhang, F. Pan, Y. A. Luo, Y. X. Liu, and J. P. Draayer, Phys. Rev. C **86**, 044312 (2012).
[27] F. Iachello, A. Leviatan, and D. Petrellis, Phys. Lett. B **705**, 379 (2011).
[28] R. B. Cakirli, R. F. Casten, R. Winkler, K. Blaum, and M. Kowalska, Phys. Rev. Lett. **102**, 082501 (2009).
[29] L. K. Peker and J. K. Tuli, Nucl. Data Sheets **82**, 187 (1997).
[30] N. Nica, Nucl. Data Sheets **110**, 749 (2009).
[31] M. R. Bhat, Nucl. Data Sheets **89**, 797 (2000).
[32] B. Singh, Nucl. Data Sheets **102**, 1 (2004).
[33] E. derMateosian and J. K. Tuli, Nucl. Data Sheets **75**, 827 (1995).
[34] B. Singh, Nucl. Data Sheets **80**, 263 (1997).
[35] A. Artna-Cohen, Nucl. Data Sheets **79**, 1 (1996).
[36] R. G. Helmer, Nucl. Data Sheets **107**, 507 (2006).
[37] C. W. Reich and R. G. Helmer, Nucl. Data Sheets **85**, 171 (1998).
[38] C. W. Reich, Nucl. Data Sheets **104**, 1 (2005).
[39] C. W. Reich, Nucl. Data Sheets **99**, 753 (2003).
[40] R. G. Helmer, Nucl. Data Sheets **103**, 565 (2004).
[41] R. F. Casten, M. Wilhelm, E. Radermacher, N. V. Zamfir, and P. von Brentano, Phys. Rev. C **57**, R1553 (1998).
[42] N. V. Zamfir *et al.*, Phys. Rev. C **60**, 054312 (1999).
[43] P. E. Garrett *et al.*, Phys. Rev. Lett. **103**, 062501 (2009).
[44] K. Heyde, J. Jolie, R. Fossion, S. De Baerdemacker, and V. Hellemans, Phys. Rev. C **69**, 054304 (2004).
[45] K. Heyde and J. L. Wood, Rev. Mod. Phys. **83**, 1467 (2011).
[46] J. Jolie, P. Cejnar, and J. Dobeš, Phys. Rev. C **60**, 061303(R) (1999).

[47] M. E. Bunker and C. W. Reich, Rev. Mod. Phys. **43**, 348 (1971).
[48] R. F. Casten, D. D. Warner, D. S. Brenner, and R. L. Gill, Phys. Rev. Lett. **47**, 1433 (1981).
[49] D. Petrelli, A. Leviatan, and F. Iachello, Ann. Phys. (NY) **326**, 926 (2011).
[50] A. Leviatan, D. Petrelli, and F. Iachello, *Proceedings of the 14th Int. Symposium on Capture Gamma-Ray Spectroscopy and Related Topics (CGS14), Guelph, Canada, 2011* (World Scientific, Singapore, 2012).
[51] F. Iachello and P. Van Isacker, *Interacting Boson-Fermion Model* (Cambridge University Press, Cambridge, 1991).
[52] J. Jolie, S. Heinze, P. Van Isacker, and R. F. Casten, Phys. Rev. C **70**, 011305(R) (2004).
[53] C. E. Alonso, J. M. Arias, L. Fortunato, and A. Vitturi, Phys. Rev. C **72**, 061302(R) (2005).
[54] C. E. Alonso, J. M. Arias, and A. Vitturi, Phys. Rev. C **75**, 064316 (2007).
[55] C. E. Alonso, J. M. Arias, L. Fortunato, and A. Vitturi, Phys. Rev. C **79**, 014306 (2009).
[56] M. Böyükata, C. E. Alonso, J. M. Arias, L. Fortunato, and A. Vitturi, Phys. Rev. C **82**, 014317 (2010).
[57] J. Barea, C. E. Alonso, and J. M. Arias, Phys. Rev. C **83**, 024307 (2011).